



CHORUS

This is the accepted manuscript made available via CHORUS. The article has been published as:

Braiding of Majorana-like corner states in electric circuits and its non-Hermitian generalization

Motohiko Ezawa

Phys. Rev. B **100**, 045407 — Published 10 July 2019

DOI: [10.1103/PhysRevB.100.045407](https://doi.org/10.1103/PhysRevB.100.045407)

Braiding of Majorana-like corner states in electric circuits and its non-Hermitian generalization

Motohiko Ezawa

Department of Applied Physics, University of Tokyo, Hongo 7-3-1, 113-8656, Japan

The braiding is a key for topological quantum computations. Such a proposal has been made based on Majorana fermions. In this paper, it is shown that the braiding behavior is simulated in electric circuits by constructing Majorana-like corner states. First, we simulate the Kitaev model by an LC electric circuit and the $p_x + ip_y$ model by an LC circuit together with operational amplifiers. Zero-energy edge states emerge in the topological phase, which are detectable by measuring impedance. Next, we simulate the Bernevig-Hughes-Zhang model by including an effective magnetic field without breaking the particle-hole symmetry, where zero-energy corner states emerge in the topological phase. It is demonstrated that they are Ising anyons subject to the braiding. Namely we derive $\sigma^2 = -1$ for them, where σ denotes the single-exchange operation. We also study non-Hermitian generalizations of these models by requiring the particle-hole symmetry. It is shown that the braiding holds also in certain reciprocal non-Hermitian generalizations.

I. INTRODUCTION

A Majorana fermion will be a key for future topological quantum computations¹ owing to the braiding. Majorana fermions are realized in topological superconductors²⁻⁴ and Kitaev spin liquids^{5,6}. In these systems, the particle-hole symmetry (PHS) plays an essential role since the zero-energy states become Majorana fermions⁷⁻⁹. Recently, Majorana fermions are realized as corner states in various systems¹⁰⁻¹⁶, for some of which the braiding has already been shown^{15,16}. Furthermore, Majorana fermions in non-Hermitian systems have been studied in various contexts¹⁷⁻²⁶. It is an interesting problem to seek other systems exhibiting Majorana-like braiding behavior. Especially, it is fascinating if such states can be simulated by electric circuits.

Needless to say, electric circuits are classical systems and they cannot describe fermions. In general, the Hamiltonian density is of the form $\hat{H}(\mathbf{k}) = \Psi^\dagger(\mathbf{k})H(\mathbf{k})\Psi(\mathbf{k})$ in condensed matter physics, where $\Psi(\mathbf{k})$ is the electron annihilation operator. It is customary to refer to $H(\mathbf{k})$ also as the Hamiltonian. Topological properties of the system is actually determined by the property of $H(\mathbf{k})$. It is intriguing that^{27,28}, when the system parameters are appropriately chosen, the circuit Laplacian has the same expression as the Hamiltonian $H(\mathbf{k})$, although this Hamiltonian does not give the time evolution of the circuit. A topological phase transition is induced by tuning variable capacitors and inductors, where the topological and trivial phases are distinguishable by the bulk-edge correspondence as in the case of condensed matter physics. The edge and corner states are observed by measuring the impedance²⁷⁻³⁴. In this way, various topological phases have been simulated by electric circuits, such as the Su-Schrieffer-Heeger model (SSH) model²⁸, graphene^{28,30}, Weyl semimetal^{28,35}, nodal-line semimetal^{36,37}, higher-order topological phases^{27,29,32}, Chern insulators³¹ and non-Hermitian topological phases^{33,34}.

In this paper, we make a first step to simulate the braiding behavior of Majorana fermions in electric circuits by using Majorana-like corner states. First, we construct the Kitaev model either by a pure LC circuit or by an LC circuit together with operational amplifiers. Next, the $p_x + ip_y$ model is constructed by aligning these two circuits along the orthogonal

directions. Then, using these circuits as building blocks, we simulate the Bernevig-Hughes-Zhang (BHZ) model together with an effective Zeeman field by an electric circuit. The model corresponds to a second-order topological superconductor with the emergence of a pair of Majorana corner states. Zero-energy edge or corner states are well observed by measuring the impedance in these models. Although the braiding is predicted in the Kitaev model⁴, it is not easy to simulate it in electric circuits. Here, we demonstrate explicitly that the braiding behavior is found between a pair of corner states in the BHZ model by calculating the Berry phase in an electric circuit.

The introduction of resistance makes the electric circuit non-Hermitian due to the Joule loss³³. There are two types of non-Hermitian models, i.e., reciprocal models and nonreciprocal models, where nonreciprocity indicates that the forward and backward hopping amplitudes are different between two nodes. As far as the PHS is respected, it is shown that the braiding holds for the two corner states also in a reciprocal non-Hermitian extension of the BHZ model. The braiding becomes meaningless in the nonreciprocal extension.

II. THE KITAEV MODEL AND ELECTRIC-CIRCUIT SIMULATION

The Kitaev p -wave topological superconductor model is the fundamental model hosting Majorana zero-energy edge states in one dimensional (1D) space. The model is represented in the two forms, i.e., by the Hamiltonian \hat{H}^y with the imaginary superconducting pairing, and \hat{H}^x with the real superconducting pairing. They are given by

$$\hat{H}^i(\mathbf{k}) = \Psi^\dagger(\mathbf{k})H^i(\mathbf{k})\Psi(\mathbf{k}), \quad (1)$$

with the Nambu operator

$$\Psi(\mathbf{k}) = \{c(\mathbf{k}), c^\dagger(\mathbf{k})\}, \quad (2)$$

and

$$H^i(\mathbf{k}) = H_t(\mathbf{k})\sigma_z + H_\Delta^i(\mathbf{k}) \quad (3)$$

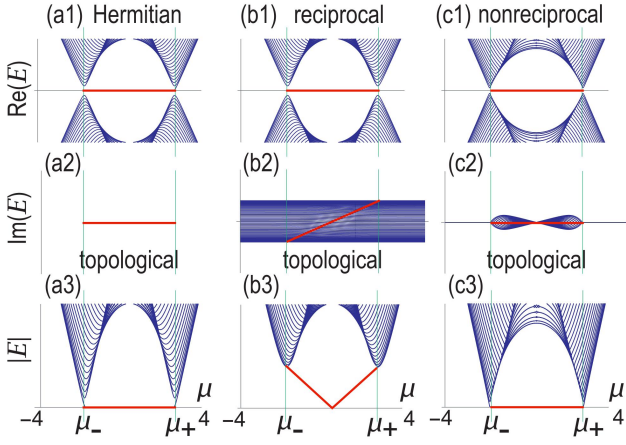


FIG. 1: Energy spectra of a finite chain of the Hermitian and non-Hermitian Kitaev models with length $N = 40$, where the red lines represent topological edge states. They emerge only in the topological phase ($\mu_- < \mu < \mu_+$) with $\mu_{\pm} = \pm|2t|$ in the Hermitian and reciprocal non-Hermitian models. The horizontal axis is the chemical potential μ . The parameters are as follows: We have chosen $t^b = t^f = 1$, $\Delta^b = \Delta^f = 0.5$ and $\mu = 0$ for the original Kitaev model (a). We have chosen the same parameters as (a) except $t^b = t^f = 1 + 0.2i$ for the reciprocal non-Hermitian Kitaev model (b). We have chosen the same parameters as (a) except $\Delta^b = 0.3$ for the nonreciprocal non-Hermitian Kitaev model (c).

in terms of the hopping term H_t and the interaction term H_{Δ}^i ,

$$H_t(\mathbf{k}) = -t \cos k - \mu, \quad (4)$$

$$H_{\Delta}^y(\mathbf{k}) = \Delta_y \sigma_y \sin k, \quad H_{\Delta}^x(\mathbf{k}) = \Delta_x \sigma_x \sin k, \quad (5)$$

where t , μ and Δ_i represent the hopping amplitude, the chemical potential and the superconducting gap parameter. It is a two-band model, and the Hamiltonian is a 2×2 matrix. It is well known that the system is topological for $|\mu| < |2t|$ and trivial for $|\mu| > |2t|$ irrespective of Δ_i provided $\Delta_i \neq 0$, as is demonstrated in Fig.1 based on the bulk-edge correspondence.

We simulate the Kitaev Hamiltonian (3) by electric circuits. There are two types of circuits corresponding to the two Hamiltonians H^y and H^x , as illustrated in Fig.2(a) and (b).

Let us explain how to construct electric circuits for them: See Fig.2. We use two main wires to represent a two-band model: One wire consists of capacitors C in series, implementing the electron band, while the other wire consists of inductors L in series, implementing the hole band. The hopping parameters are opposite between the electron and hole bands, which are represented by capacitors and inductors. Indeed, they contribute the terms proportional to $i\omega C$ and $1/(i\omega L)$ to the circuit Laplacian $J_{ab}(\omega)$ in (7), respectively, where ω is the frequency of the AC current.

In the wire with capacitors (inductors), each node a is connected to the ground via an inductor L_0 (C_0), as in Fig.2(a)–(b). This setting is made to make the system topological.

We then introduce pairing interactions between them. In order to construct the model H^y , we cross bridge two wires by capacitors C_X and inductors L_X as shown in Fig.2(a).

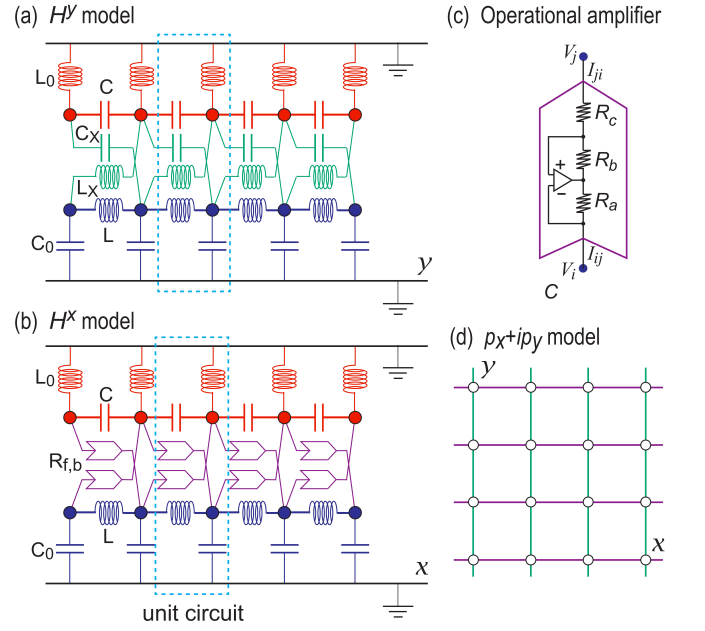


FIG. 2: Minimal electronic circuits simulating the Kitaev model. Each circuit consists of two main wires colored in red and blue, simulating electron and hole bands, respectively. The unit cell is shown by a dotted cyan box, and contains two nodes colored in red and blue. (a) The H^y model is realized by a pure LC circuit. (b) The H^x model is realized by an additional use of operational amplifiers. (c) Structure of an operational amplifier. (d) The $p_x + ip_y$ model is constructed so that the 1D circuits (a) and (b) are aligned in the x and y directions, respectively. Green and purple links represent pairing interactions of the types (a) and (b), respectively.

On the other hand, in order to construct the model H^x , we cross bridge two wires by operational amplifiers, which act as negative impedance converters with current inversion³¹. In the operational amplifier, the resistance depends on the current flowing direction; R_f for the forward flow and $-R_b$ for the backward flow with the convention that $R_b > 0$. We set $R_X = R_f = R_b$ to make the system reciprocal. A generalization to the nonreciprocal theory with $R_f \neq R_b$ is discussed in Section V.

The unit cell indicated by a dotted cyan box contains two sites in Fig.2. Accordingly, we set

$$I_a = (I_a^L, I_a^C), \quad V_a = (V_a^L, V_a^C), \quad (6)$$

where $I_a^{L(C)}$ is the current between node $a^{L(C)}$ and the ground via the inductance L (conductance C), and $V_a^{L(C)}$ is the voltage at node $a^{L(C)}$.

When we apply an AC voltage $V(t) = V(0)e^{i\omega t}$, the Kirchoff current law leads to the following formula^{27,28},

$$I_a(\omega) = \sum_b J_{ab}(\omega) V_b(\omega), \quad (7)$$

where the sum is taken over all adjacent nodes b , and $J_{ab}(\omega)$ is called the circuit Laplacian.

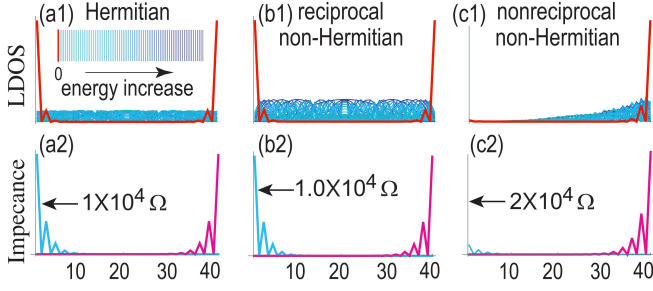


FIG. 3: (a1)–(c1) LDOS of a finite chain of the Hermitian and non-Hermitian Kitaev models with length $N = 40$ in the topological phase, where the red peaks at the edges represent zero-energy edge states. Skin states are observed in the nonreciprocal system (c1). The energy of the state is represented by a color subject to the color palette in the inset of (a1). (a2)–(c2) Two-point impedance of the corresponding LC circuit with operational amplifiers, where the peaks at the edges are due to zero-energy edge states. The horizontal axis is the site index. Magenta (cyan) curves indicate the impedance when one node is fixed at the left (right) edge. The parameters are as follows: $t = 1$, $\Delta = 0.5$ and $\mu = 0$ for the Kitaev model (a); $t = 1 + 0.2i$, $\Delta = 0.5$ and $\mu = 0$ for the reciprocal non-Hermitian Kitaev model (b); $t = 1$, $\Delta^f = 0.5$, $\Delta^b = 0.3$ and $\mu = 0$ for the nonreciprocal non-Hermitian Kitaev model (c).

(i) In the case of the circuit in Fig.2(a) we explicitly obtain

$$J = \begin{pmatrix} f_1 & g_1 \\ g_2 & f_2 \end{pmatrix}, \quad (8)$$

where

$$\begin{aligned} f_1 &= -2C \cos k + 2C - (\omega^2 L_0)^{-1}, \\ f_2 &= 2(\omega^2 L)^{-1} \cos k - 2(\omega^2 L)^{-1} + C_0, \\ g_1 &= -C_X e^{ik} + (\omega^2 L_X)^{-1} e^{-ik}, \\ g_2 &= (\omega^2 L_X)^{-1} e^{ik} - C_X e^{-ik}, \end{aligned} \quad (9)$$

describing the H^y model.

(ii) In the case of the circuit in Fig.2(b) we explicitly obtain (8), where f_1 and f_2 are given by (9) but

$$g_1 = g_2 = (i\omega R_b)^{-1} e^{ik} - (i\omega R_f)^{-1} e^{-ik}, \quad (10)$$

describing the H^x model.

The key procedure in simulation is to equate the circuit Laplacian (8) with the Hamiltonian (3). In so doing, it is necessary to require the PHS for the circuit, which requires us to tune the parameters to satisfy

$$\omega_0 \equiv 1/\sqrt{LC} = 1/\sqrt{L_0 C_0} = 1/\sqrt{L_X C_X}, \quad (11)$$

and set the AC frequency as $\omega = \omega_0$. At this frequency, we may set

$$J_{ab}(\omega) = i\omega H_{ab}^i(\omega), \quad (12)$$

which leads to

$$t = -C, \quad \mu = -2C + C_0, \quad \Delta_y = C_X, \quad \Delta_x = \frac{1}{\omega_0 R_X}, \quad (13)$$

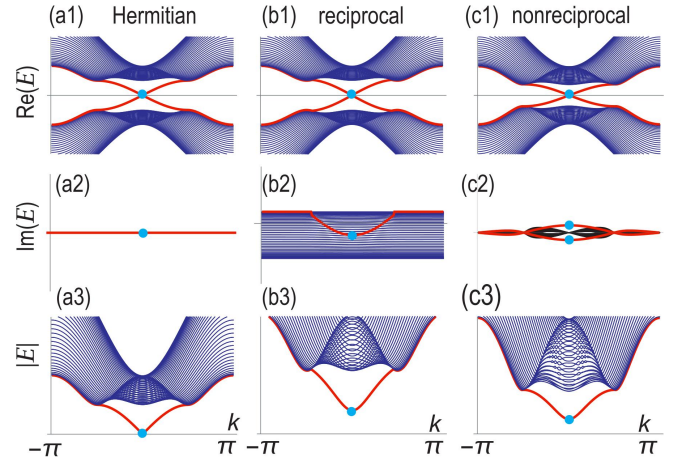


FIG. 4: Energy spectra of a nanoribbon of the Hermitian and non-Hermitian $p_x + ip_y$ models with width 40 in the topological phase, where red curves represent chiral edge states, while cyan disks represent the topological edge states. The parameters are as follows: We have chosen $t^b = t^f = 1$ and $\Delta^b = \Delta^f = 0.5$ for the original $p_x + ip_y$ model (a). We have chosen the same parameters as (a) except $t^b = t^f = 1 + 0.2i$ for the reciprocal non-Hermitian $p_x + ip_y$ model (b). We have chosen the same parameters as (a) except $\Delta^b = 0.25$ for the nonreciprocal non-Hermitian $p_x + ip_y$ model (c). We have set $\mu = 1$.

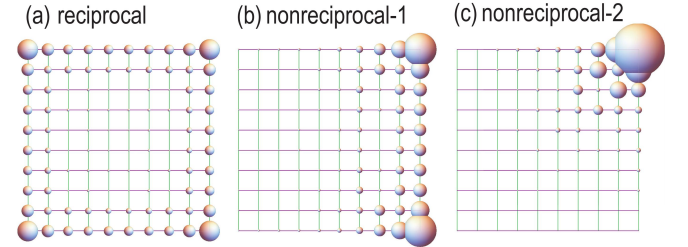


FIG. 5: LDOS of the topological edge states in the $p_x + ip_y$ model. The size of a ball represents the magnitude of LDOS. (a) The original $p_x + ip_y$ model with $\Delta_x^b = \Delta_x^f = \Delta_y^b = \Delta_y^f = 0.5$. (b) Nonreciprocal non-Hermitian $p_x + ip_y$ model with $\Delta_x^f = \Delta_y^b = \Delta_y^f = 0.5$ and $\Delta_x^b = 0.25$. Skin edge states are realized. (c) Nonreciprocal non-Hermitian $p_x + ip_y$ model with $\Delta_x^f = \Delta_y^f = 0.5$ and $\Delta_x^b = \Delta_y^b = 0.25$. Second-order corner states are realized. We have set $t_x^b = t_x^f = t_y^b = t_y^f = 1$ and $\mu = 1$ for all cases.

dictating the correspondence between the Hamiltonian model and the circuit.

The system is precisely at the topological phase-transition point $|\mu| = |2t|$ without the capacitors C_0 and the inductors L_0 , since the condition $\mu = -2t$ is satisfied. It is topological in the presence of C_0 and L_0 . The system turns into a trivial phase when we exchange the capacitors C_0 and inductors L_0 connected to ground.

By calculating the LDOS as in Fig.3(a1), we find the emergence of the zero-energy edge states in the topological phase. They are observable by measuring the impedance between the a and b nodes, which is given by³⁰ $Z_{ab} \equiv V_a/I_b = G_{ab}$, where G is the Green function defined by the inverse of the

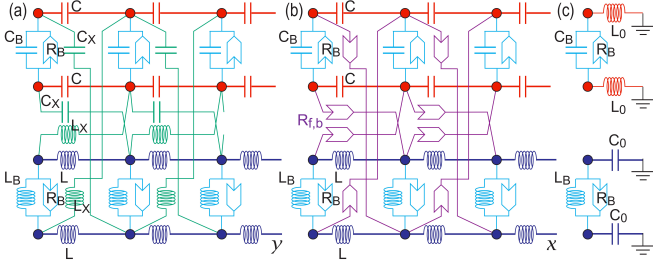


FIG. 6: Electric-circuit realization of the BHZ model together with effective field B . The B field is simulated by parts involving (C_B, R_B) and (L_B, R_B) colored in cyan. (a) 2D view into the x direction. (b) 2D view into the y direction. (c) Each node is connected to the ground by an inductor or a capacitor in (a) and (b). We have set $t = 1, \mu = 1, \Delta = 1$ and $B = 1/2$.

Laplacian $J, G \equiv J^{-1}$. We show numerical results in Fig.3(a2) for typical values of parameters, where we have set one node at the left or right edge. The behavior of the impedance is very similar to that of the LDOS. We may explicitly check that the impedance peaks are absent in the trivial phase, showing that the bulk-edge correspondence holds also in electric circuits.

III. THE $p_x + ip_y$ MODEL AND ELECTRIC-CIRCUIT SIMULATION

We next consider the $p_x + ip_y$ model, whose Hamiltonian is given by (3) with

$$H_t = t(\cos k_x + \cos k_y) - \mu, \quad (14)$$

$$H_{SC} = \Delta(\sigma_x \sin k_x + \sigma_y \sin k_y). \quad (15)$$

The model is simulated by layering the circuit for H^y in the x direction and the circuit for H^x in the y direction as shown in Fig.2(d). The relations between the parameters are given by

$$t = -C, \quad \mu = -2C + C_0, \quad \Delta = C_X = (\omega_0 R_X)^{-1}. \quad (16)$$

It is topological for $|\mu| < |2t|$, where the zero-energy edge states emerge along all four edges, as is demonstrated in Fig.4.

We show the LDOS of the topological corner states in Fig.5. In the original $p_x + ip_y$ model, the chiral edge states emerge as shown in Fig.5(a). When there is nonreciprocity along the x axis but reciprocal along the y axis, 1D skin edge states emerge as shown in Fig.5(b). On the other hand, when both the x and y axes are nonreciprocal, the second-order skin-edge states^{33,34,38} emerge as shown in Fig.5(c), where the LDOS has a strong peak at one corner.

IV. MAJORANA-LIKE CORNER STATES AND BRAIDING BEHAVIOR

It is not easy to simulate the braiding of the zero-energy edge states of the Kitaev model⁴ in the electric-circuit formalism. On the other hand, the zero-energy edge states are 1D

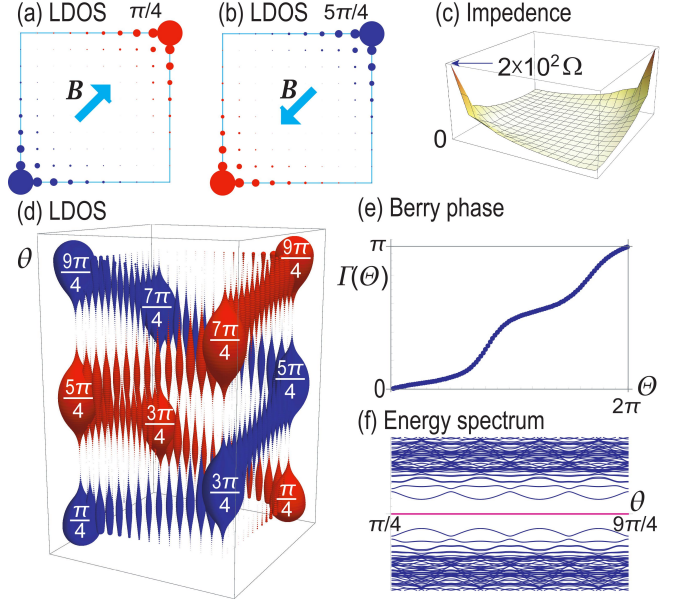


FIG. 7: LDOS of the corner states (a) at $\theta = \pi/4$ and (b) at $\theta = 5\pi/4$. These two are related by a single-exchange operation. Cyan arrows show the direction of the B field. (c) Impedance is the same at $\theta = \pi/4$ and $5\pi/4$. (d) LDOS of the corner states for $\pi/4 < \theta < 9\pi/4$, and their braiding. (e) Evolution of the Berry phase towards a double-exchange operation. (f) Energy spectrum evolution during the braiding. The corner states in red remains to be separated from the bulk spectrum in blue.

objects in the $p_x + ip_y$ model. We proceed to investigate a 2D model possessing a pair of zero-energy corner states to explore the braiding.

Such a model is given by the Bernevig-Hughes-Zhang (BHZ) Hamiltonian³⁹,

$$H^{\text{BHZ}} = H_t \tau_z + H_{\text{SO}} \tau_x, \quad (17)$$

where H_t and H_{SO} are given by (14) and (15), respectively. Although it is proposed for a topological insulator, it has the PHS, $\Xi^{-1} H(\mathbf{k}) \Xi = -H(-\mathbf{k})$ with $\Xi = \tau_y \sigma_y K$, where K represents complex conjugation. When the Zeeman term

$$H_Z = B(\sigma_x \cos \theta + B \sigma_y \sin \theta) \quad (18)$$

is applied, it becomes a second-order topological superconductor with the emergence of zero-energy topological corner states^{15,40}. However, it breaks the PHS¹³. Here we propose the term

$$H_{\tau Z} = B \tau_z (\sigma_x \cos \theta + \sigma_y \sin \theta), \quad (19)$$

which respects the PHS. Such a term does not exist in condensed matter, but it is allowed in electric circuits: See cyan parts in Fig.6.

We simulate the BHZ model with the B field by an electric circuit,

$$H_{\tau Z}^{\text{BHZ}}(\theta) \equiv H^{\text{BHZ}} + H_{\tau Z}. \quad (20)$$

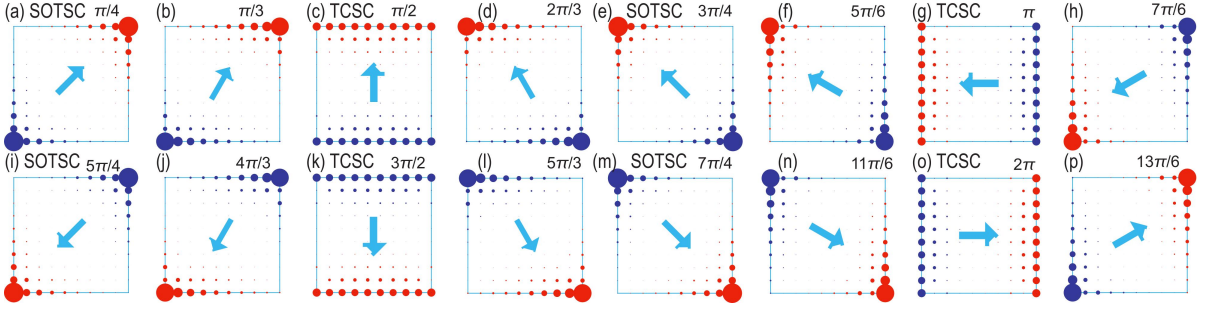


FIG. 8: LDOS for various θ . The system is a SOTSC for $\theta = \pi/4, 3\pi/4, 5\pi/4$ and $7\pi/4$. It is a TCSC for $\theta = \pi/2, \pi, 3\pi/2$ and 2π .

We may use the circuits for the Kitaev model (Fig.2) as building blocks to construct the circuits for the BHZ model as in Fig.6. Since it is a four-band model, we use four main wires. By analyzing the Kirchhoff current law, we may derive the circuit Laplacian $J_{ab}(\omega)$, which is now a 4×4 matrix. Solving

$$J_{ab}(\omega) = i\omega H_{\tau Z}^{\text{BHZ}}, \quad (21)$$

we obtain the correspondence between the system parameters. They are given by (16) supplemented by $B_x = C_B$ or L_B and $B_y = R_B$ for the B field. We show the LDOS and the impedance at $\theta = \pi/4, 5\pi/4$ in Fig.7(a)–(c), where the zero-energy corner states are clearly observed. See the LDOS at other values of θ in Fig.8.

The zero-energy corner states subject to the PHS are Majorana states in condensed matter physics. Majorana fermions are known to be Ising anyons possessing the property $\sigma^2 = -1$, where σ denotes the single-exchange operation^{1,5}. It is well known that only fermions and bosons are possible in 3D, for which $\sigma^2 = 1$. On the other hand, anyons are possible only in 2D. We recognize that this anyonic property is most important as a characteristics of Majorana fermions for future application to topological quantum computers.

Since the electric circuits are classical system, the corner states obtained in electric circuits cannot be Majorana fermions. Furthermore, we cannot discuss half quantization of the corner states. Nevertheless, as we now show, the same braiding behavior as the Majorana fermions is found for the corner states based on the adiabatic evolution of the wave functions. In this sense we may call the corner states the Majorana-like corner states.

We investigate the braiding for a pair of corner states. By increasing θ continuously from $\pi/4$ to $5\pi/4$ ($9\pi/4$), we can exchange the position of two corner states once (twice) as in Fig.7(d). The corner states remain to be zero-energy states with a finite gap during the process, as shown in Fig.7(f). Thus, they remain well separated from the bulk bands during the exchange of the two corner states. The key property is how the wave function changes as θ increases. Note that the phase of the wave function is observable by the phase shift in the electric circuit.

We start with an eigenstate $|\psi_\beta(\pi/4)\rangle$ of $H_{\tau Z}^{\text{BHZ}}(\theta)$ at $\theta = \pi/4$, which describes a pair of corner states as in Fig.8(a). Such corner states are selectively excited at the resonant frequency ω , as can be demonstrated by the emergence of the

impedance resonance. We then increase θ adiabatically. The wave function $|\psi_\alpha(\theta)\rangle$ develops as^{1,5,41}

$$|\psi_\alpha(\theta)\rangle = \sum_{\beta=1,2} e^{i\Gamma_{\alpha\beta}(\Theta)} |\psi_\beta(\pi/4)\rangle, \quad (22)$$

where $\Theta = \theta - \pi/4$, and $\Gamma_{\alpha\beta}(\Theta)$ is the Berry phase,

$$\Gamma_{\alpha\beta}(\Theta) = i \int_{\pi/4}^{\pi/4+\Theta} \langle \psi_\alpha(\theta) | \partial_\theta | \psi_\beta(\theta) \rangle d\theta. \quad (23)$$

There are two-fold degenerate zero-energy corner states at $\theta = \pi/4$. Since these two states are well separated as in Fig.7(a), we may label them by $\alpha = 1, 2$. Furthermore, we may construct the eigenfunctions continuous in θ such that $\langle \psi_\alpha(\theta) | \psi_\beta(\theta) \rangle = \delta_{\alpha\beta}$ for any value of θ . Then, it follows that $\Gamma_{\alpha\beta}(\Theta)$ is diagonal; $\Gamma(\Theta) \equiv \Gamma_{11}(\Theta) = \Gamma_{22}(\Theta)$. We show a numerical result for $\Gamma(\Theta)$ in Fig.7(e). In particular, we obtain $\Gamma(2\pi) = \pi$.

We have investigated the BHZ model together with the B field. In condensed matter physics, the role of the B field is to turn a topological superconductor with the zero-energy edge states into a second order topological superconductor (TOTSC) with the zero-energy corner states^{15,40}. We have used the magnetic field B in the previous work⁴⁰. Now in the present work we may control it by tuning the values of capacitors and so on in electric circuits. We show the LDOS at various values of the angle θ in Fig.8. It is found that the system corresponds to a SOTSC for $\theta = \pi/4, 3\pi/4, 5\pi/4, 7\pi/4$, and to a topological crystalline superconductor (TCSC) for $\theta = \pi/2, \pi, 3\pi/2, 2\pi$ in condensed matter physics.

The single and double exchanges correspond to the rotations $\Theta = \pi$ and $\Theta = 2\pi$, respectively. After the double exchange we obtain $\Gamma_{\alpha\beta}(2\pi) = \pi\delta_{\alpha\beta}$, which yields $|\psi_1\rangle \rightarrow -|\psi_1\rangle$ and $|\psi_2\rangle \rightarrow -|\psi_2\rangle$, or $\sigma^2 = -1$. Consequently, the braiding is satisfied by the corner states in electric circuits.

We can check that the braiding is robust against disorders. We first study the effect of disorders on the braiding in the BHZ model together with the B field. We introduce randomness into capacitors and inductors which uniformly distributing from $-V$ to V . We show that the Majorana-like corner states are robust in the presence of disorders as long as the PHS is preserved in Fig.9(a). The Majorana-like corner states are found to persist for $V \lesssim t$. In Fig.9(b), we show the angle

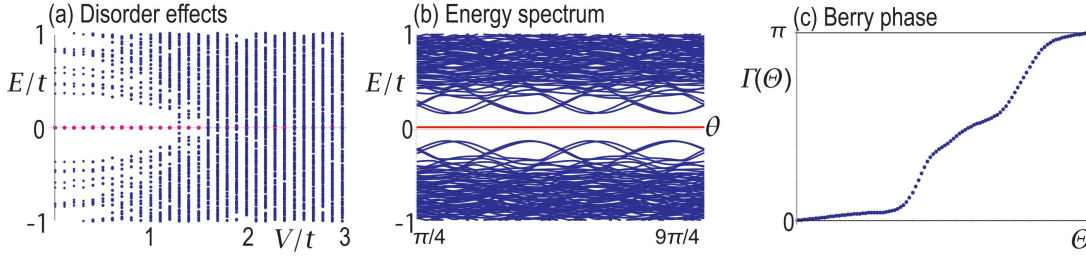


FIG. 9: (a) Energy spectrum as a function of the disorder strength. The zero-energy states are robust for $|V| < t$. (b) Angle dependence of the energy spectrum with disorder strength $V = 0.2t$. The zero-energy corner states are well separated from the bulk spectrum. (c) The Berry phase evolution with disorder strength $V = 0.2t$. It is quantized even in the presence of the disorder.

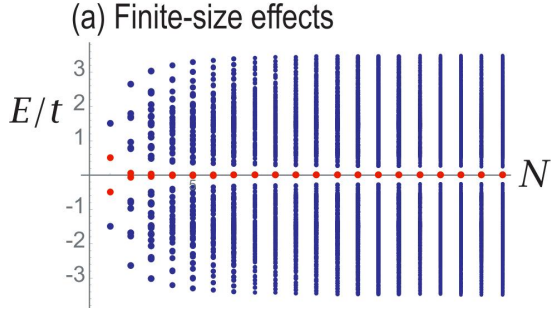


FIG. 10: Energy spectrum as a function of the system size N . The degenerate zero-energy states emerge for $N > 4$.

dependence of the energy spectrum in the presence of disorders. As a result, the Berry phase remains to be quantized even in the presence of disorders as shown in Fig.9(c).

We next study the effect of the system size in the BHZ model together with the B field. In Fig.10 we show the energy spectrum as a function of the system size N . The corner states are not degenerate at $E = 0$ for $N = 1, 2, 3$. The energy decreases exponentially first, and they are degenerate at $E = 0$ for $N \geq 4$. Consequently, the braiding holds for the corner states in electric circuits whose size is as small as $N = 4$.

V. NON-HERMITIAN MAJORANA-LIKE STATES

A non-Hermitian model is either reciprocal or nonreciprocal. To make the analysis concrete, we explicitly consider a non-Hermitian Kitaev model respecting the PHS. The Hamiltonian (3) together with (4) and (5) is generalized as

$$H(k) = i\gamma\mathbb{I} + \begin{pmatrix} f(t^b, t^f; k) & g(\Delta^b, \Delta^f; k) \\ g(\Delta^{b*}, \Delta^{f*}; k) & -f(t^{b*}, t^{f*}; k) \end{pmatrix}, \quad (24)$$

with

$$f(t^b, t^f; k) = t^b e^{ik} + t^f e^{-ik} - \mu, \quad (25)$$

$$g(\Delta^b, \Delta^f; k) = -i(\Delta^b e^{ik} - \Delta^f e^{-ik}), \quad (26)$$

and γ representing dissipation, where t^b (t^f) is a backward (forward) hopping amplitude, Δ^b (Δ^f) is a backward (for-

ward) superconducting pairing amplitude, and μ is the chemical potential. Parameters t^b , t^f , Δ^b and Δ^f take complex values, while μ and γ take real values. It satisfies the PHS, $\Xi^{-1}H(k)\Xi = -H(-k)$, with $\Xi = \sigma_x K$.

As derived in (A23) in Appendix, by diagonalizing (24), the bulk gap is found to close at

$$|\mu| = |\text{Re}(t^b + t^f) \pm |\Delta^b - \Delta^f||. \quad (27)$$

Gap-closing points are not phase-transition points when skin edge states are present in non-Hermitian theory^{33,38,42-47}.

We seek for topological phases. The system remains to be in the class Z_2 even for the non-Hermitian system⁴⁸, and hence, the topological number is given by the Z_2 invariant ν in the original Kitaev model as

$$(-1)^\nu = -\text{sgn}[H_z(0)H_z(\pi)], \quad (28)$$

where H_z is the coefficient of σ_z by expanding H as $H(k) = \sum_{\alpha=0,x,y,z} H_\alpha(k)\sigma_\alpha$, and $k = 0, \pi$ are the PHS invariant momenta. The formula (28) is valid also for the non-Hermitian system because of the PHS. Calculating it explicitly we find that

$$(-1)^\nu = \text{sgn} \left[[\text{Re}(t^b + t^f)]^2 - \mu^2 \right], \quad (29)$$

where we have used the fact that $H_z(k)$ is real at the PHS invariant momenta because of the condition $H_z(k) = H_z^*(-k)$ required by the PHS²⁶.

It follows from (29) that there are two phases with the phase-transition points $\mu_\pm = \pm |\text{Re}(t^b + t^f)|$. The system has a line gap⁴⁸ separating the valence and conduction bands. The system is topological ($\nu = 1$) for $|\mu| < |\text{Re}(t^b + t^f)|$ and trivial ($\nu = 0$) for $|\mu| > |\text{Re}(t^b + t^f)|$. The justification of (29) as the topological number is made by confirming numerically the non-Hermitian bulk-edge correspondence^{33,43-47} inherent to nonreciprocal systems. The gap-closing points (27) become identical to the topological phase-transition points μ_\pm when the system is reciprocal, $\Delta^b = \Delta^f$.

We study two characteristic cases of non-Hermitian models: (i) Topological edge states with pure imaginary energy emerge in a reciprocal non-Hermitian model [Fig.1(b)], when we assume a complex value for the hopping amplitude $t^b = t^f$ and a real value for the pairing amplitude $\Delta^b = \Delta^f$. (ii)

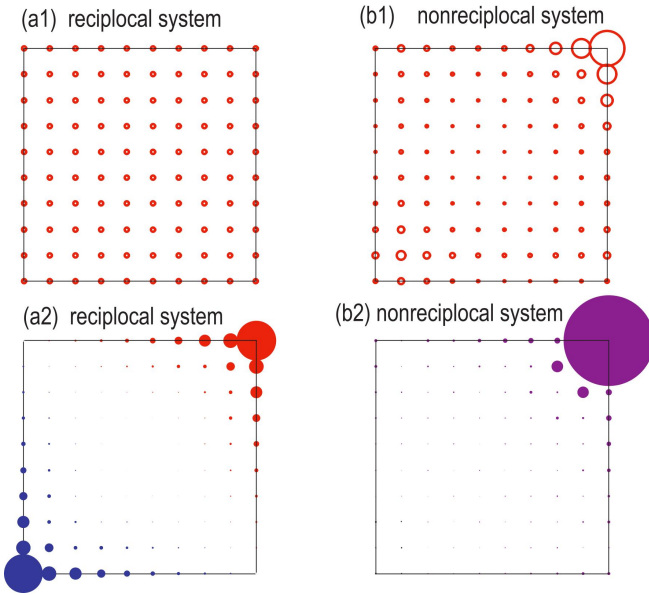


FIG. 11: LDOS for the BHZ model. (a1) LDOS for all states in reciprocal system. (a2) LDOS for the Majorana-like corner states in reciprocal system. (b1) LDOS for all states in nonreciprocal system. (b2) LDOS for the zero-energy corner states in nonreciprocal system. We have set $R_X = R_\Delta = 0.2$. Skin states are observed for the nonreciprocal system.

Topological edge states with zero energy emerge in a non-reciprocal non-Hermitian model [Fig.1(c)], when we assume a real value for the hopping amplitudes $t^b = t^f$ and real values for the pairing amplitudes but with $\Delta^b \neq \Delta^f$

The LDOS is shown for all eigen-energies in Fig.3(a1)–(c1) by taking typical values of sample parameters in the Hermitian, reciprocal non-Hermitian and nonreciprocal non-Hermitian cases. The characteristic feature of the nonreciprocal non-Hermitian model is the emergence of skin edge states as in [Fig.3(c1)], where all the eigen states are localized at one edge, as was first found in the non-Hermitian SSH^{43–45}. Namely, two topological edge states are mixed between themselves and furthermore they are mixed with the bulk states in the vicinity of one edge. This is also the case for the topological corner states in the nonreciprocal non-Hermitian BHZ model as in Fig.11. The braiding becomes meaningless in the nonreciprocal non-Hermitian models because there are no separated corner states.

We may construct a reciprocal non-Hermitian model respecting the PHS, by inserting a resistor R to a capacitance C and an inductor L in series in Fig.6. The circuit Laplacian is obtained just by replacing

$$C \rightarrow \frac{1}{1/C + i\omega R}, \quad \frac{1}{\omega^2 L} \rightarrow \frac{1}{\omega^2 L - i\omega R}. \quad (30)$$

As we show in (A58) and (A59) in Appendix, the resultant non-Hermitian model is different from the original Hermitian model only by a pure imaginary shift. In such a case the braiding holds just as it is since the wave functions are not modified.

We simulate the non-Hermitian Kitaev model (3) by electric circuits. There are two types of circuits corresponding to the two Hamiltonians H^y and H^x , as illustrated in Fig.2(a) and (b). The correspondence between the parameters of the Hamiltonian and those of the circuit Laplacian is given by (A57) in Appendix.

A similar argument is applicable also for the BHZ model. See Fig.11. We find that Majorana-like corner states emerge as in Fig.11(a2) in these types of reciprocal non-Hermitian systems, for which the braiding holds. On the other hand, the skin corner states appear in nonreciprocal non-Hermitian systems as in Fig.11(b2), for which the braiding of a pair of corner states does not make sense.

VI. DISCUSSION

We have made a first step to simulate the braiding behavior of Majorana fermions in electric circuits by using Majorana-like corner states in the BHZ model. We have explicitly revealed an anyonic property of Majorana-like corner states. Corner states emerge in electric circuits whose size is as small as $N = 4$, which is a benefit on future high-density applications. Furthermore, various extensions are possible to electric circuits for such as the dimerized Kitaev model⁴⁹ and the Kitaev ladder model⁵⁰. Our results might open a new way for topological quantum computations based on braiding in electric circuits.

Acknowledgements

The author is very grateful to A. Kurobe for fruitful conversations on the subject, which motivated the present work. He is also thankful to Y. Tanaka and N. Nagaosa for helpful discussions on the subject. He also thanks to T. Pahomi and A. A. Soluyanov on discussions on the braiding of Majorana states. This work is supported by the Grants-in-Aid for Scientific Research from MEXT KAKENHI (Grants No. JP17K05490, No. JP15H05854 and No. JP18H03676). This work is also supported by CREST, JST (JPMJCR16F1 and JPMJCR1874).

Appendix A: Non-Hermitian generalization of various formulas

1. Particle-hole symmetry

The particle-hole symmetry (PHS) is defined by

$$\Xi^{-1} H(k) \Xi = -H(-k) \quad (\text{A1})$$

with the eigen equation

$$H(k) |\psi\rangle = E(k) |\psi\rangle. \quad (\text{A2})$$

It is generalized to the non-Hermitian theory just as it is. We find

$$H(k) \Xi |\psi\rangle = -\Xi H(-k) |\psi\rangle = -\Xi E(-k) |\psi\rangle = -E^*(-k) \Xi |\psi\rangle, \quad (\text{A3})$$

and thus

$$H(k) |\phi\rangle = -E^*(-k) |\phi\rangle, \quad |\phi\rangle = \Xi |\psi\rangle. \quad (\text{A4})$$

The wave functions always appear in pairs with respect to the energy ($E(k)$, $-E^*(-k)$). When $E = -E^*$ at the PHS invariant momentum, only one Majorana state emerges. The condition is that the energy is zero or pure imaginary.

The BdG Hamiltonian can be expanded in terms of the Pauli matrices as

$$H(k) = \sum_{\alpha=0,x,y,z} H_{\alpha}(k) \sigma_{\alpha}. \quad (\text{A5})$$

It follows from (A1) that²⁶

$$H_0(k) = -H_0^*(-k), \quad H_x(k) = -H_x^*(-k), \quad H_y(k) = -H_y^*(-k), \quad H_z(k) = H_z^*(-k) \quad (\text{A6})$$

in the presence of the PHS.

2. Derivation of non-Hermitian Kitaev models with the PHS

The most general extension of the Kitaev model is given by

$$H(k) = \begin{pmatrix} t_1^b e^{ik} + t_1^f e^{-ik} - \mu + V & \frac{1}{i} (\Delta_1^b e^{ik} - \Delta_1^f e^{-ik}) \\ \frac{1}{i} (\Delta_2^b e^{ik} - \Delta_2^f e^{-ik}) & -t_2^b e^{ik} - t_2^f e^{-ik} + \mu + V \end{pmatrix}. \quad (\text{A7})$$

This Hamiltonian is non-Hermitian and nonreciprocal in general. It is reduced to the original Kitaev model for real $t \equiv t_{1,2}^b = t_{1,2}^f$, complex $\Delta \equiv \Delta_{1,2}^b = \Delta_{1,2}^f$ and $V = 0$. Note that the present model is different from the non-Hermitian Kitaev model with the PT symmetry^{19,20,25}, where the chemical potential is complex.

The particle-hole conjugate of the Hamiltonian is

$$\Xi^{-1} H(k) \Xi = \begin{pmatrix} -t_2^{b*} e^{-ik} - t_2^{f*} e^{ik} + \mu^* + V^* & \frac{1}{i} (\Delta_2^{f*} e^{ik} - \Delta_2^{b*} e^{-ik}) \\ \frac{1}{i} (\Delta_1^{f*} e^{ik} - \Delta_1^{b*} e^{-ik}) & t_1^{b*} e^{-ik} + t_1^{f*} e^{ik} - \mu^* + V^* \end{pmatrix}, \quad (\text{A8})$$

where $\Xi = \sigma_x K$ is the PHS operator and K represents the complex conjugation. On the other hand, we have

$$-H(-k) = \begin{pmatrix} -t_1^b e^{-ik} - t_1^f e^{ik} + \mu - V & -\frac{1}{i} (\Delta_1^b e^{-ik} - \Delta_1^f e^{ik}) \\ -\frac{1}{i} (\Delta_2^b e^{-ik} - \Delta_2^f e^{ik}) & t_2^b e^{-ik} + t_2^f e^{ik} - \mu - V \end{pmatrix}. \quad (\text{A9})$$

The PHS imposes the condition

$$P^{-1} H(k) P = -H(-k), \quad (\text{A10})$$

which leads to the following relations,

$$t_1^b = t_2^{b*} \equiv t^b, \quad t_1^f = t_2^{f*} \equiv t^f, \quad \Delta_1^b = \Delta_2^{b*} \equiv \Delta^b, \quad \Delta_1^f = \Delta_2^{f*} \equiv \Delta^f, \quad \mu = \mu^*, \quad V = -V^*. \quad (\text{A11})$$

Thus, the non-Hermitian particle-hole symmetric Kitaev model is generally written in the form of

$$H(k) = i\gamma\mathbb{I} + \begin{pmatrix} t^b e^{ik} + t^f e^{-ik} - \mu & \frac{1}{i} (\Delta^b e^{ik} - \Delta^f e^{-ik}) \\ \frac{1}{i} (\Delta^{b*} e^{ik} - \Delta^{f*} e^{-ik}) & -t^{b*} e^{ik} - t^{f*} e^{-ik} + \mu \end{pmatrix} \quad (\text{A12})$$

where we have set $V = i\gamma$ with γ being real. The components in the expansion (A5) read

$$H_x(k) = \text{Re}\Delta^b \sin k - \text{Re}\Delta^f \sin k - i(\text{Re}\Delta^b \cos k - \text{Re}\Delta^f \cos k), \quad (\text{A13})$$

$$H_y(k) = -\text{Im}\Delta^b \sin k + \text{Im}\Delta^f \sin k + i(\text{Im}\Delta^b \cos k - \text{Im}\Delta^f \cos k), \quad (\text{A14})$$

$$H_z(k) = e^{ik} \text{Re}t^b + e^{-ik} \text{Re}t^f - \mu, \quad (\text{A15})$$

$$H_0(k) = ie^{ik} \text{Im}t^b + ie^{-ik} \text{Im}t^f + i\gamma. \quad (\text{A16})$$

The energy is given by

$$E = H_0 \pm \sqrt{\text{Re}H \cdot \text{Re}H - \text{Im}H \cdot \text{Im}H + 2i\text{Re}H \cdot \text{Im}H}, \quad (\text{A17})$$

where $A \cdot B = \sum_{i=x,y,z} A_i B_i$. It is explicitly obtained as

$$E(k) = i\gamma + e^{ik} \text{Im}t^b + e^{-ik} \text{Im}t^f \pm \sqrt{G}, \quad (\text{A18})$$

with

$$G(k) = \left[\mu - (e^{ik} \text{Re}t^b + e^{-ik} \text{Re}t^f)^2 \right]^2 + (\Delta^b e^{ik} - \Delta^f e^{-ik}) (\Delta^{b*} e^{ik} - \Delta^{f*} e^{-ik}). \quad (\text{A19})$$

The degeneracy of the eigenvalues requires

$$\text{Re}H \cdot \text{Re}H = \text{Im}H \cdot \text{Im}H, \quad \text{Re}H \cdot \text{Im}H = 0. \quad (\text{A20})$$

Especially, the energy at the PHS invariant momentum is given by

$$E^\pm(0) = i\gamma + \text{Im}t^b + \text{Im}t^f \pm \sqrt{\left[\mu - [\text{Re}(t^b + t^f)]^2 \right]^2 - |\Delta^b - \Delta^f|^2}, \quad (\text{A21})$$

$$E^\pm(\pi) = i\gamma - \text{Im}t^b - \text{Im}t^f \pm \sqrt{\left[\mu + [\text{Re}(t^b + t^f)]^2 \right]^2 - |\Delta^b - \Delta^f|^2}. \quad (\text{A22})$$

By solving $E^+(0) = E^-(0)$ and $E^+(\pi) = E^-(\pi)$, the bulk gap is found to close at

$$|\mu| = |\text{Re}(t^b + t^f) \pm |\Delta^b - \Delta^f||. \quad (\text{A23})$$

This is the phase transition point (27) in the main text.

3. Derivation of the non-Hermitian $p_x + ip_y$ model with the PHS

The most general extension of the $p_x + ip_y$ model is given by

$$H(k) = \begin{pmatrix} t_{1x}^b e^{ik_x} + t_{1x}^f e^{-ik_x} + t_{1y}^b e^{ik_y} + t_{1y}^f e^{-ik_y} - \mu + V, & \frac{1}{i} (\Delta_{1x}^b e^{ik_x} - \Delta_{1x}^f e^{-ik_x}) - (\Delta_{1y}^b e^{ik_y} - \Delta_{1y}^f e^{-ik_y}) \\ \frac{1}{i} (\Delta_{2x}^b e^{ik_x} - \Delta_{2x}^f e^{-ik_x}) + (\Delta_{2y}^b e^{ik_y} - \Delta_{2y}^f e^{-ik_y}), & -t_{2x}^b e^{ik_x} - t_{2x}^f e^{-ik_x} - t_{2y}^b e^{ik_y} - t_{2y}^f e^{-ik_y} + \mu + V \end{pmatrix}. \quad (\text{A24})$$

Its particle-hole conjugate is calculated as

$$\begin{aligned} & \Xi^{-1} H(k) \Xi \\ &= \begin{pmatrix} -t_{2x}^{b*} e^{-ik_x} - t_{2x}^{f*} e^{ik_x} - t_{2y}^{b*} e^{-ik_y} - t_{2y}^{f*} e^{ik_y} + \mu^* + V^*, & \frac{1}{i} (\Delta_{2x}^{f*} e^{ik_x} - \Delta_{2x}^{b*} e^{-ik_x}) - (\Delta_{2y}^{f*} e^{ik_y} - \Delta_{2y}^{b*} e^{-ik_y}) \\ \frac{1}{i} (\Delta_{1x}^{f*} e^{ik_x} - \Delta_{1x}^{b*} e^{-ik_x}) + (\Delta_{1y}^{f*} e^{ik_y} - \Delta_{1y}^{b*} e^{-ik_y}), & t_{1x}^{b*} e^{-ik_x} + t_{1x}^{f*} e^{ik_x} + t_{1y}^{b*} e^{-ik_y} + t_{1y}^{f*} e^{ik_y} - \mu^* + V^* \end{pmatrix}, \end{aligned} \quad (\text{A25})$$

where $\Xi = \sigma_x K$ is the particle-hole symmetry operator and K represents the complex conjugation. On the other hand, we have

$$-H(-k) = \begin{pmatrix} -t_{1x}^b e^{-ik_x} - t_{1x}^f e^{ik_x} - t_{1y}^{b*} e^{-ik_y} + t_{1y}^{f*} e^{ik_y} + \mu - V & -\frac{1}{i} \left(\Delta_{1x}^b e^{-ik_x} - \Delta_{1x}^f e^{ik_x} \right) + \left(\Delta_{1y}^b e^{-ik_y} - \Delta_{1y}^f e^{ik_y} \right) \\ -\frac{1}{i} \left(\Delta_{2x}^b e^{-ik_x} - \Delta_{2x}^f e^{ik_x} \right) - \left(\Delta_{2y}^b e^{-ik_y} - \Delta_{2y}^f e^{ik_y} \right) & t_{2x}^b e^{-ik_x} + t_{2x}^f e^{ik_x} + t_{2y}^b e^{-ik_y} + t_{2y}^f e^{ik_y} - \mu - V \end{pmatrix}. \quad (\text{A26})$$

The particle-hole symmetry imposes the condition

$$P^{-1} H(k) P = -H(-k). \quad (\text{A27})$$

In order to satisfy the PHS, the following relations are required,

$$t_{1x}^b = t_{2x}^{b*} \equiv t_x^b, \quad t_{1x}^f = t_{2x}^{f*} \equiv t_x^f, \quad t_{1y}^b = t_{2y}^{b*} \equiv t_y^b, \quad t_{1y}^f = t_{2y}^{f*} \equiv t_y^f, \quad (\text{A28})$$

$$\Delta_{1x}^b = \Delta_{2x}^{b*} \equiv \Delta_x^b, \quad \Delta_{1x}^f = \Delta_{2x}^{f*} \equiv \Delta_x^f, \quad \Delta_{1y}^b = \Delta_{2y}^{b*} \equiv \Delta_y^b, \quad \Delta_{1y}^f = \Delta_{2y}^{f*} \equiv \Delta_y^f, \quad (\text{A29})$$

$$\mu = \mu^*, \quad V = -V^*. \quad (\text{A30})$$

Thus, the non-Hermitian particle-hole symmetric $p_x + ip_y$ model is generally written in the form of

$$H(k) = i\gamma \mathbb{I} + \begin{pmatrix} t_x^b e^{ik_x} + t_x^f e^{-ik_x} + t_y^b e^{ik_y} + t_y^f e^{-ik_y} - \mu & \frac{1}{i} \left(\Delta_x^b e^{ik_x} - \Delta_x^f e^{-ik_x} \right) - \left(\Delta_y^b e^{ik_y} - \Delta_y^f e^{-ik_y} \right) \\ \frac{1}{i} \left(\Delta_x^{b*} e^{ik_x} - \Delta_x^{f*} e^{-ik_x} \right) + \left(\Delta_y^{b*} e^{ik_y} - \Delta_y^{f*} e^{-ik_y} \right) & -t_x^{b*} e^{ik_x} - t_x^{f*} e^{-ik_x} - t_y^{b*} e^{ik_y} - t_y^{f*} e^{-ik_y} + \mu \end{pmatrix}, \quad (\text{A31})$$

where

$$H_z(k) = e^{ik_x} \text{Ret}_x^b + e^{-ik_x} \text{Ret}_x^f + e^{ik_y} \text{Ret}_y^b + e^{-ik_y} \text{Ret}_y^f - \mu. \quad (\text{A32})$$

It is summarized as

$$H(k) = i\gamma \mathbb{I} + \begin{pmatrix} f(t_x^b, t_x^f, t_y^b, t_y^f) & g(\Delta_x^b, \Delta_x^f, \Delta_y^b, \Delta_y^f) \\ g(\Delta_x^{b*}, \Delta_x^{f*}, -\Delta_y^{b*}, -\Delta_y^{f*}) & -f(t_x^{b*}, t_x^{f*}, t_y^{b*}, t_y^{f*}) \end{pmatrix}, \quad (\text{A33})$$

with

$$f(t_x^b, t_x^f, t_y^b, t_y^f) = t_x^b e^{ik_x} + t_x^f e^{-ik_x} + t_y^b e^{ik_y} + t_y^f e^{-ik_y} - \mu, \quad (\text{A34})$$

$$g(\Delta_x^b, \Delta_x^f, \Delta_y^b, \Delta_y^f) = -i(\Delta_x^b e^{ik_x} - \Delta_x^f e^{-ik_x}) - (\Delta_y^b e^{ik_y} - \Delta_y^f e^{-ik_y}). \quad (\text{A35})$$

The energy at the PHS invariant momenta read

$$E(0,0) = i\gamma + \text{Im} \left(t_x^b + t_x^f + t_y^b + t_y^f \right) \pm \sqrt{\left[\mu - \left[\text{Re} \left(t_x^b + t_x^f + t_y^b + t_y^f \right) \right]^2 \right]^2 - \left| \Delta_x^b - \Delta_x^f - i \left(\Delta_y^b - \Delta_y^f \right) \right|^2}, \quad (\text{A36})$$

$$E(\pi,\pi) = i\gamma - \text{Im} \left(t_x^b + t_x^f + t_y^b + t_y^f \right) \pm \sqrt{\left[\mu - \left[\text{Re} \left(t_x^b + t_x^f + t_y^b + t_y^f \right) \right]^2 \right]^2 - \left| \Delta_x^b - \Delta_x^f - i \left(\Delta_y^b - \Delta_y^f \right) \right|^2}, \quad (\text{A37})$$

$$E(0,\pi) = i\gamma + \text{Im} \left(t_x^b + t_x^f - t_y^b - t_y^f \right) \pm \sqrt{\left[\mu - \left[\text{Re} \left(t_x^b + t_x^f - t_y^b - t_y^f \right) \right]^2 \right]^2 - \left| \Delta_x^b - \Delta_x^f + i \left(\Delta_y^b - \Delta_y^f \right) \right|^2}, \quad (\text{A38})$$

$$E(\pi,0) = i\gamma + \text{Im} \left(-t_x^b - t_x^f + t_y^b + t_y^f \right) \pm \sqrt{\left[\mu - \left[\text{Re} \left(-t_x^b - t_x^f + t_y^b + t_y^f \right) \right]^2 \right]^2 - \left| \Delta_x^b - \Delta_x^f + i \left(\Delta_y^b - \Delta_y^f \right) \right|^2}. \quad (\text{A39})$$

By solving $E^+(0,0) = E^-(0,0)$, $E^+(\pi,\pi) = E^-(\pi,\pi)$, $E^+(0,\pi) = E^-(0,\pi)$, $E^+(\pi,0) = E^-(\pi,0)$, the bulk gap is found to close at

$$|\mu| = \left| \text{Re} \left(t_x^b + t_x^f \pm \eta_t \left(t_y^b + t_y^f \right) \right) + \left| \Delta_x^b - \Delta_x^f - i\eta_t \left(\Delta_y^b - \Delta_y^f \right) \right| \right|, \quad (\text{A40})$$

with $\eta_t = \pm 1$ and $\eta_\Delta = \pm 1$. On the other hand, the topological number (8) is calculated as

$$\begin{aligned} w &= \frac{1}{2} \left(\text{sgn} [H_z(0,0)] + \text{sgn} [H_z(\pi,\pi)] - \text{sgn} [H_z(0,\pi)] - \text{sgn} [H_z(\pi,0)] \right) \\ &= \frac{1}{2} \text{sgn} [\text{Ret}_x^b + \text{Ret}_x^f + \text{Ret}_y^b + \text{Ret}_y^f - \mu] + \frac{1}{2} \text{sgn} [-\text{Ret}_x^b - \text{Ret}_x^f - \text{Ret}_y^b - \text{Ret}_y^f - \mu] \\ &\quad - \frac{1}{2} \text{sgn} [\text{Ret}_x^b + \text{Ret}_x^f - \text{Ret}_y^b - \text{Ret}_y^f - \mu] - \frac{1}{2} \text{sgn} [-\text{Ret}_x^b - \text{Ret}_x^f + \text{Ret}_y^b + \text{Ret}_y^f - \mu]. \end{aligned} \quad (\text{A41})$$

The system remains to be in the class Z even for the non-Hermitian case⁴⁸. Then the topological number is given by the Chern number w in the original $p_x + ip_y$ model. It is evaluated as

$$w = \frac{1}{2}(\text{sgn}[H_z(0,0)] + \text{sgn}[H_z(\pi,\pi)] - \text{sgn}[H_z(0,\pi)] - \text{sgn}[H_z(\pi,0)]), \quad (\text{A42})$$

where $(k_x, k_y) = (0,0), (0,\pi), (\pi,0)$ and (π,π) are the PHS invariant momenta. This formula is valid also for the non-Hermitian system because of the PHS. Calculating (A42) explicitly we find that the topological phase transition occurs at

$$\mu_{\pm}^1 = \pm \text{Re} |t_x^b + t_x^f + t_y^b + t_y^f|, \quad \mu_{\pm}^2 = \pm \text{Re} |t_x^b + t_x^f - t_y^b - t_y^f|. \quad (\text{A43})$$

The formula (A42) is justified to define the topological number by confirming numerically the non-Hermitian bulk-edge correspondence. Indeed, the topological edge states emerge only in the topological phase for nanoribbon geometry. We show the chiral edge states in the topological phase in Fig.4, where non-Hermitian topological edge states are found to emerge at a pure-imaginary energy. The phase transition point (A43) is different from the bulk-gap closing point (A40) as a characteristic feature of skin edge states.

4. Non-Hermitian terms induced by resistance

We consider the case where resistors are sequentially connected to capacitors or inductors. Then, it is enough to make the replacement (30) or

$$C \rightarrow \frac{1}{1/C + i\omega R}, \quad \frac{1}{\omega^2 L} \rightarrow \frac{1}{\omega^2 L - i\omega R}. \quad (\text{A44})$$

We consider the circuit Laplacian (8) or

$$J = \begin{pmatrix} f_1 & g_1 \\ g_2 & f_2 \end{pmatrix}. \quad (\text{A45})$$

We find that the diagonal terms become

$$f_1 = -\frac{2}{1/C + i\omega R} \cos k + \frac{2}{1/C + i\omega R} - \frac{1}{\omega^2 L_0 - i\omega R_0}, \quad (\text{A46})$$

$$f_2 = \frac{2}{\omega^2 L - i\omega R} \cos k - \frac{2}{\omega^2 L - i\omega R} + \frac{1}{1/C_0 + i\omega R_0}. \quad (\text{A47})$$

With respect to the off-diagonal terms we find

$$g_1 = -\frac{1}{1/C_X + i\omega R_X} e^{ik} + \frac{1}{\omega^2 L_X - i\omega R_X} e^{-ik}, \quad (\text{A48})$$

$$g_2 = \frac{1}{\omega^2 L_X - i\omega R_X} e^{ik} - \frac{1}{1/C_X + i\omega R_X} e^{-ik} \quad (\text{A49})$$

for the H^y model, and

$$g \equiv g_1 = g_2 = \frac{1}{i\omega R_b} e^{ik} - \frac{1}{i\omega R_f} e^{-ik} = \frac{1}{i\omega (R + R_\Delta)} e^{ik} - \frac{1}{i\omega (R - R_\Delta)} e^{-ik} \quad (\text{A50})$$

for the H^x model, where we have defined

$$R \equiv \frac{R_b + R_f}{2}, \quad R_\Delta \equiv \frac{R_b - R_f}{2} \quad (\text{A51})$$

At the resonance frequency ($\omega = 1/\sqrt{LC}$), they read

$$f_1 = -\frac{2}{1/C + iR/\sqrt{LC}} \cos k + \frac{2}{1/C + iR/\sqrt{LC}} - \frac{1}{1/C_0 - iR_0/\sqrt{LC}}, \quad (\text{A52})$$

$$f_2 = \frac{2}{1/C - iR/\sqrt{LC}} \cos k - \frac{2}{1/C - iR/\sqrt{LC}} + \frac{1}{1/C_0 + iR_0/\sqrt{LC}}, \quad (\text{A53})$$

and

$$g_1 = -\frac{1}{1/C_X + iR_X/\sqrt{LC}}e^{ik} + \frac{1}{1/C_X - iR_X/\sqrt{LC}}e^{-ik}, \quad (\text{A54})$$

$$g_2 = \frac{1}{1/C_X - iR_X/\sqrt{LC}}e^{ik} - \frac{1}{1/C_X + iR_X/\sqrt{LC}}e^{-ik}, \quad (\text{A55})$$

and

$$g = \frac{1}{i(R + R_\Delta)/\sqrt{LC}}e^{ik} - \frac{1}{i(R - R_\Delta)/\sqrt{LC}}e^{-ik}. \quad (\text{A56})$$

The system parameters are renormalized as

$$t = -\frac{2/C}{1/C^2 + R^2/LC}, \quad \mu = \frac{2/C}{1/C^2 + R^2/LC} - \frac{1/C_0}{1/C_0^2 + R_0^2/LC}, \quad \Delta = \frac{1/C_X}{1/C_X^2 + R_X^2/LC}. \quad (\text{A57})$$

As a result, the additional terms to the Kitaev model with H^y are given by

$$\Delta H = i \left[\frac{2R/\sqrt{LC}}{1/C^2 + R^2/LC} \begin{pmatrix} 1 - \cos k & 0 \\ 0 & 1 - \cos k \end{pmatrix} - \frac{R_0/\sqrt{LC}}{1/C_0^2 + R_0^2/LC} \begin{pmatrix} 1 & 0 \\ 0 & 1 \end{pmatrix} + \frac{R_X/\sqrt{LC}}{1/C_X^2 + R_X^2/LC} \begin{pmatrix} 0 & \cos k \\ \cos k & 0 \end{pmatrix} \right], \quad (\text{A58})$$

while those with H are given by

$$\Delta H \simeq i \left[\frac{2R/\sqrt{LC}}{1/C^2 + R^2/LC} \begin{pmatrix} 1 - \cos k & 0 \\ 0 & 1 - \cos k \end{pmatrix} - \frac{R_0/\sqrt{LC}}{1/C_0^2 + R_0^2/LC} \begin{pmatrix} 1 & 0 \\ 0 & 1 \end{pmatrix} + \frac{R_\Delta}{R^2/\sqrt{LC}} \begin{pmatrix} 0 & \cos k \\ \cos k & 0 \end{pmatrix} \right] \quad (\text{A59})$$

for small R_Δ . These terms are the non-Hermitian corrections to the Hermitian theory due to the resistors.

The additional terms ΔH are diagonal for $R_X = 0$ and $R_\Delta = 0$, where the Hamiltonian only shifts the energy in the pure imaginary direction. In this case, the wave function does not change and the Berry phase remains as it is in the Hermitian model. On the other hand, once $R_X \neq 0$ or $R_\Delta \neq 0$, the system becomes nonreciprocal and the skin states emerge.

-
- ¹ C. Nayak, S. H. Simon, A. Stern, M. Freedman, and S. Das Sarma, Rev. Mod. Phys. **80**, 1083 (2008).
² X.-L. Qi, S.-C. Zhang, Rev. Mod. Phys. **83**, 1057 (2011).
³ M. Sato and Y. Ando, Rep. Prog. Phys. **80**, 076501 (2017).
⁴ J. Alicea, Y. Oreg, G. Refael, F. von Oppen and M.P.A. Fisher, Nat. Phys. **7**, 412 (2011).
⁵ A. Kitaev, Annals of Physics **321**, 2 (2006).
⁶ Y. Kasahara, T. Ohnishi, Y. Mizukami, O. Tanaka, Sixiao Ma, K. Sugii, N. Kurita, H. Tanaka, J. Nasu, Y. Motome, T. Shibauchi, Y. Matsuda, Nature **559**, 227 (2018).
⁷ J. Alicea, Rep. Prog. Phys. **75**, 076501 (2012).
⁸ C. W.J. Beenakker, Annu. Rev. Condens. Matter Phys. **4**, 113 (2013).
⁹ S.R. Elliott and M. Franz, Rev. Mod. Phys. **87**, 137 (2015).
¹⁰ Z. Yan, F. Song, Z. Wang, Phys. Rev. Lett. **121**, 096803 (2018).
¹¹ Q. Wang, C.-C. Liu, Y.-M. Lu, F. Zhang, Phys. Rev. Lett. **121**, 186801 (2018).
¹² Y. Volpez, D. Loss, J. Klinovaja, Phys. Rev. Lett. **122**, 126402 (2019).
¹³ Y. Wang, M. Lin, T. L. Hughes, Phys. Rev. B **98**, 165144 (2018).
¹⁴ T. Liu, J. J. He, F. Nori, Phys. Rev. B **98**, 245413 (2018).
¹⁵ X. Zhu, Phys. Rev. B **97**, 205134 (2018).
¹⁶ T. E. Pahomi, M. Sigrist, A. A. Soluyanov, cond-mat/arXiv:1904.07822
¹⁷ S. Malzard, C. Poli, H. Schomerus, Phys. Rev. Lett. **115**, 200402 (2015).
¹⁸ P. San-Jose, J. Cayao, E. Prada and R. Aguado, Scientific Reports **6**, 21427 (2016).
¹⁹ C. Yuze, Phys. Rev. A **93**, 062130 (2016).
²⁰ C. Li, Liang, Jin, Z. Song, cond-mat/arXiv:1710.07794.
²¹ C. Li, X. Z. Zhang, G. Zhang, Z. Song, Phys. Rev. B **97**, 115436 (2018).
²² E. Cobanera, A. Alase, G. Ortiz, L. Viola, Phys. Rev. B **98**, 245423 (2018).
²³ A. A. Zyuzin, P. Simon, Phys. Rev. B **99**, 165145 (2019).
²⁴ J. Avila, F. Penaranda, E. Prada, P. San-Jose, R. Aguado, cond-mat/arXiv:1807.04677
²⁵ K. Kawabata, Y. Ashida, H. Katsura, M. Ueda, Phys. Rev. B **98**, 085116 (2018).
²⁶ K. Kawabata, S. Higashikawa, Z. Gong, Y. Ashida, M. Ueda, Nat. Commun. **10**, 297 (2019).
²⁷ S. Imhof, C. Berger, F. Bayer, J. Brehm, L. Molenkamp, T. Kiessling, F. Schindler, C. H. Lee, M. Greiter, T. Neupert, R. Thomale, Nat. Phys. **14**, 925 (2018).
²⁸ C. H. Lee, S. Imhof, C. Berger, F. Bayer, J. Brehm, L. W. Molenkamp, T. Kiessling and R. Thomale, Communications Physics, **1**, 39 (2018).
²⁹ M. Serra-Garcia, R. Susstrunk and S. D. Huber, Phys. Rev. B **99**, 020304 (2019).
³⁰ T. Helbig, T. Hofmann, C. H. Lee, R. Thomale, S. Imhof, L. W.

- Molenkamp and T. Kiessling, Phys. Rev. B **99**, 161114 (2019).
- ³¹ T. Hofmann, T. Helbig, C. H. Lee, M. Greiter, R. Thomale, arXiv:1809.08687.
- ³² M. Ezawa, Phys. Rev. B **98**, 201402(R) (2018).
- ³³ M. Ezawa, Phys. Rev. B **99**, 201411(R) (2019)
- ³⁴ M. Ezawa, Phys. Rev. B **99**, 121411(R) (2019).
- ³⁵ Y. Lu, N. Jia, L. Su, C. Owens, G. Juzeliunas, D. I. Schuster and J. Simon, Phys. Rev. B **99**, 020302 (2019).
- ³⁶ K. Luo, R. Yu and H. Weng, Research (2018), ID 6793752.
- ³⁷ K. Luo, J. Feng, Y. X. Zhao, and R. Yu, cond-mat/arXiv:1810.09231.
- ³⁸ C. H. Lee, L. Li and J. Gong, cond-mat/arXiv:1810.11824.
- ³⁹ B. A. Bernevig, T. L. Hughes, and S.-C. Zhang, Science **314**, 1757 (2006).
- ⁴⁰ M. Ezawa, Phys. Rev. Lett. **121**, 116801 (2018).
- ⁴¹ S. D. Sarma, M. Freedman, and C. Nayak, npj Quantum Inf. **1**, 15001 (2015).
- ⁴² Y. Xiong, J. Physics Communications **2**, 035043 (2018).
- ⁴³ S. Yao and Z. Wang, Phys. Rev. Lett. **121**, 086803 (2018).
- ⁴⁴ S. Yao, F. Song and Z. Wang, Phys. Rev. Lett. **121**, 136802 (2018).
- ⁴⁵ F. K. Kunst, E. Edvardsson, J. C. Budich and E. J. Bergholtz, Phys. Rev. Lett. **121**, 026808 (2018).
- ⁴⁶ C. H. Lee, R. Thomale, Phys. Rev. B **99**, 201103(R) (2019).
- ⁴⁷ L. Jin and Z. Song, Phys. Rev. B **99**, 081103 (2019).
- ⁴⁸ K. Kawabata, K. Shiozaki, M. Ueda, M. Sato, cond-mat/arXiv:1812.09133
- ⁴⁹ R. Wakatsuki, M. Ezawa, Y. Tanaka and N. Nagaosa, Phys. Rev. B **90**, 014505 (2014).
- ⁵⁰ R. Wakatsuki, M. Ezawa, N. Nagaosa, Phys. Rev. B **89**, 174514 (2014).